Nature of the Active Sites for CO Reduction on Copper Nanoparticles; Suggestions for Optimizing Performance

Tao Cheng, Hai Xiao, and William A. Goddard*

Materials and Process Simulation Center (MSC) and Joint Center for Artificial Photosynthesis (JCAP), California Institute of Technology, Pasadena, California 91125, United States

S Supporting Information

ABSTRACT: Recent experiments show that the grain boundaries (GBs) of copper nanoparticles (NPs) lead to an outstanding performance in reducing CO_2 and CO to alcohol products. We report here multiscale simulations that simulate experimental synthesis conditions to predict the structure of a 10 nm Cu NP (158 555 atoms). To identify active sites, we first predict the CO binding at a large number of sites and select four exhibiting CO binding stronger than the (211) step surface. Then, we predict the formation energy of the *OCCOH intermediate as a descriptor for C−C coupling, identifying two active sites, both of which have an under-coordinated surface square site adjacent to a subsurface stacking fault. We then propose a periodic Cu surface (4 by 4 supercell) with a similar site that substantially decreases the formation energy of *OCCOH, by 0.14 eV.

An efficient means of reducing CO_2 to fuels or hydrocarbon feedstocks would provide an artificial means for closing the entire carbon cycle, offering ways for improving energy and environmental sustainability.[1,2] Indeed, reducing CO_2 to methane (CH_4) or ethylene (C_2H_4) is thermodynamically feasible, with a standard reduction potential of 0.17 and 0.08 V, respectively, versus the reversible hydrogen electrode (RHE) at pH 6.8.[3] However, the extremely sluggish reaction kinetics and lack of selectivity associated with these reactions pose a significant challenge for catalyst design.

Copper (Cu) is the only metal catalyst that reduces CO_2 into significant amounts of hydrocarbons.[4] Since the pioneering work of Hori et al., the catalytic performance and reaction mechanism of CO_2 reduction reaction (CO_2RR) on metallic copper has been studied extensively, both experimentally[3−5] and theoretically.[6−9] However, metallic copper catalysts remain far from technical requirements. Typically, commercial electrolyzers operate with over 70% efficiency at current densities above 200 mAcm^{-2},[10] while the best CO_2 electrolyzers operate below 20 mAcm^{-2}.[11] An additional disadvantage of the copper catalyst is the polydispersity of the products: up to 14 different products have been identified to accompany major hydrocarbon products, which significantly decreases the Faraday efficiency.[3]

It is accepted that the rate-determining step (RDS) for CO_2RR is carbon monoxide (CO) reduction,[12] based on experiments showing that the CO reduction reaction (CORR) and CO_2RR have similar overpotential and product distribu-

tions.[13,14] Indeed our previous QM metadynamics calculations found that the free energy barrier at 298 K for the RDS from CO_2 to CO (0.43 eV)[8] on Cu(100) is lower than the free energy barrier of RDS from CO to CH_4 (0.96 eV)[15,16] or the free energy barrier of RDS from CO to C_2H_4 (0.69 eV)[15] at pH 7. Therefore, the technical difficulties in CO_2RR are mostly associated with CORR.

Significant progress has been made in improving CORR efficiency using Cu nanoparticle (NP) catalysts. Thus, in 2014, Li et al. reported a nanocrystalline copper catalyst derived from cuprous oxide (Cu_2O) that reduces CO exclusively to ethanol under modest potentials (−0.25 V to −0.5 V verse RHE) in CO-saturated alkaline H_2O.[17] They speculated that the presence of highly active sites on grain boundaries (GBs) might explain the outstanding performance. This hypothesis was further supported by subsequent work of Feng et al, who found that the activity for reducing CO to ethanol or acetate was **linearly proportional to the density of GBs**.[18] Then Verdaguer-Casadevall et al. used thermogravimetric experiments to show that high CORR activity correlates with surface sites that bind CO more strongly than low-index and stepped Cu facets.[19] Unfortunately, these experiments do not provide information on the atomistic structure of these active sites. To optimize performance, we need this atomistic information.

In this work, we determine the probable atomistic structure responsible for the enhanced performance of Cu NPs using first-principles-based multiscale simulation methods. Thus, we mimic the experiment computationally to synthesize, characterize, and benchmark the performance of Cu NP catalysis. First, we "synthesize" a Cu NP on a carbon nanotube (CNT) support by simulating the chemical vapor deposition (CVD) experiment[18] using Molecular Dynamics (MD) simulations with the embedded-atom model (EAM).[20] To keep close to the experimental conditions, we used an 8.39 nm diameter single wall CNT with a 44.28 nm length as the catalysis support (the experiment uses a multiwall CNT of similar outside dimension). To simulate the CVD experiment (which uses an e-beam evaporated Cu source), we added Cu atoms into the simulation cell with a deposition rate of 3.2 Å ns^{-1} for 30 ns (the experiment deposition rate is 2 Å s^{-1} for 50 s).[18] We observed the quick development of supersaturated copper vapor that then began to condense. As the concentration of Cu vapor reached 0.5 Cu atom/nm^3, we observed the formation of 23 Cu atom nucleus on the CNT surface that proliferated in

various directions until the boundaries met. After 30 ns, we obtained a coarse Cu NP on CNT with a nominal thickness of about 10 nm, which is consistent with the experimental catalyst.[18]

We employed simulated annealing to heal the defects resulting from our fast deposition rate. The peak temperature in the simulated annealing is 1200 K (~100 K higher than the experimental melting point of Cu metal). Each annealing cycle contained a 10 ps heating ramp from 300 to 1200 K followed by a 5 ps NVT simulation at 1200 K, and then a 10 ps cooling ramp from 1200 to 300 K. Finally, we carried out a 15 ps NVT simulation at 300 K. After 100 such annealing cycles, we found that all grain boundaries disappeared to form a single fully crystallized Cu NP. From the annealing trajectories, we extracted a Cu NP structure that most closely resembled the experiment catalyst (this was after 38 annealing cycles).

We then carried out 20 ps of reactive dynamics at 300 K using the reactive force field that was trained to reproduce the equation of state of Cu FCC metal and geometry of graphene on the Cu (111) surface to further refine the Cu NP structure and the interface between the Cu NP and CNT support. Finally, we removed under-coordinated Cu atoms (with coordination number less than five) expected to be washed away under the experimental conditions. The final Cu NP structure consists of 158 555 atoms with a nominal thickness of 10 nm, as shown in Figure 1A.

Our predicted X-ray Powder Diffraction (XRD) patterns show the typically broadened diffraction peaks of FCC Cu (as shown in Figure 1B broadened by the small grains), which is consistent with experiment.[18]

Our predicted TEM images (Figure 1C) show the GBs in the Cu-NP, while our dislocation analysis reveals that the most abundant dislocations are 1/6 ⟨112⟩ Shockley partial dislocation, leading to stacking faults. The total length of this dislocation is 3980 Å, which corresponds to a grain density of 254 μm^{-1} according to the experiment definition.[18]

The experiment CO−Cu binding energies obtained by applying the Redhead formula using a pre-exponential factor of 10^{13} Hz[21] leads to 0.49 eV on the (111) surface, 0.53 eV on the (100) surface, and 0.61 eV on Cu (211).[22] Our plane-wave PBE DFT calculations systematically overestimate the binding energy, leading to CO binding energies of 0.78 eV on (111), 0.87 eV on (100), and 1.07 eV on (211).

Next, we calculated the binding energy of CO on 84 sites randomly selected out of 17 363 surface sites (5‰) for DFT calculations using cluster models with a cutoff of 8 Å expected to be the best balance of efficiency and accuracy (a benchmark calculation is shown in Figure S3) which we consider to provide a computational accuracy 0.02 eV.)

We consider that the above procedure provides an unbiased sampling of phase space representing the distribution of the binding energy for the whole system. The calculated binding energy distribution is shown in Figure 2. The peak at 0.78 eV is a typical adsorption energy of the (111) crystal face, which corresponds to adsorption on rhombic sites. The peak at 0.87 eV is a typical adsorption energy of the (100) crystal plane, which corresponds to adsorption on square sites. The peak at 1.07 eV corresponds to an absorption peak of the (211) plane, which can be considered as step sites. We find that 9% of the sites have stronger CO binding sites than the (211) binding energy of 1.07 eV, very close to the experiment estimate of 10%.[19]
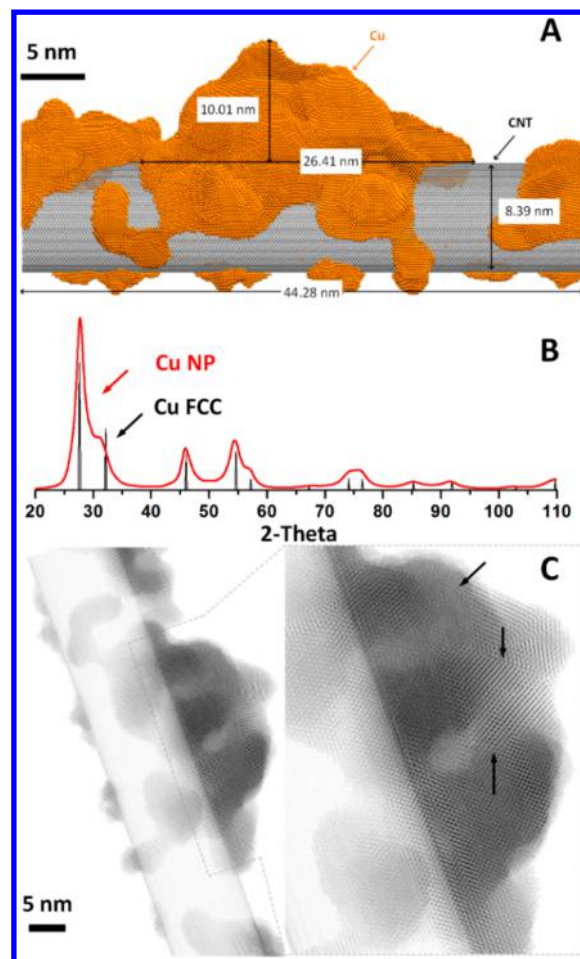
Figure 1. (A) Atomic structure of the Cu nanoparticle (NP) "synthesized" computationally by simulating the Chemical Vapor Deposition (CVD) experiment. (B) Predicted XRD diffraction pattern of the Cu-NP in A, which is compared to diffraction peaks of Cu FCC metal. (C) Predicted TEM images of the predicted Cu NP. The inset enlarges the selected area to show some of the grain boundaries (GBs).
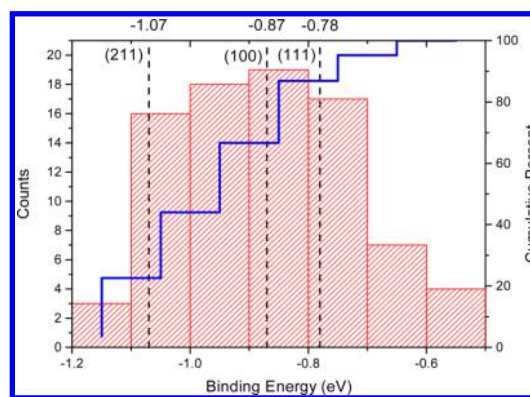
Figure 2. Distribution of CO binding energy (in eV) of Cu NP surface sites from a random sampling of 84 sites. The blue line shows the fraction of sites.

Calle-Vallejo and Koper first proposed that *OCCOH is the product of the first proton-coupled electron transfer reaction that determines the onset potential for the potential dependent step (PDS) for C2 production.[23] This prediction was supported by recent experiments by Pérez-Gallent et al., who detected a

hydrogenated dimer intermediate (*OCCOH) using Fourier transform infrared spectroscopy during CORR at low over-potentials in LiOH solutions.[24] In our recent work, we carried out full solvent QM based metadynamics to determine the RDS for C−C coupling, which we also found to be associated with the process of first electron transfer.[15,25] Consequently, we take the formation energy of *OCCOH as a descriptor to characterize the performance of surface sites toward C2 production.

The experimental work of Verdaguer et al. presented a correlation between strong CO binding sites and high CO reduction activity.[19] We took advantage of this experiment clue and focused only on sites with CO binding energy for the calculation of *OCCOH formation energy. Thus, we do the more expensive calculation of the *OCCOH formation energy only for the site with strong *CO binding.

Figure 3A to 3D show the atomic structures of the four CO binding sites predicted to be strongest, while Figure 3E to 3H
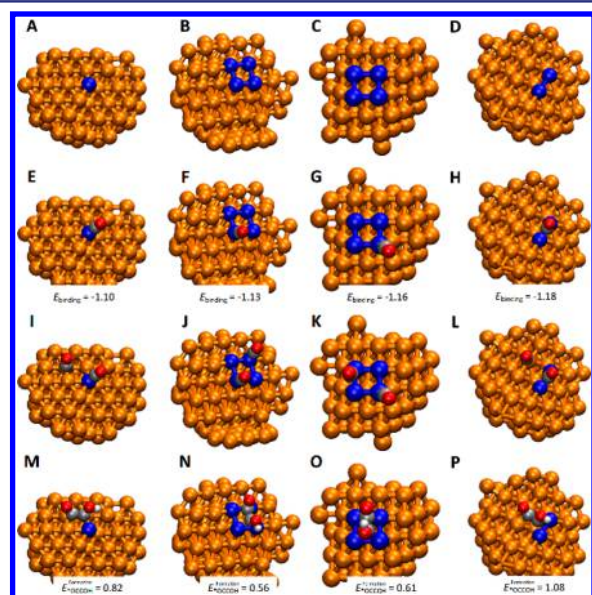
Figure 3. (A−D) Atomic structures of the four strongest CO binding sites; (E−H) the same sites with one surface bonded CO; (I−L) the same sites with two surface bonded CO; (M−P) the surface bonded *OCCOH intermediate that leads to formation of C2 products. The colors are Cu in orange, C in silver, O in red, and H in white. The closest Cu to the C is shown in blue for viewing convenience.

show the atomic configuration for binding the first CO. We carried out DFT calculations to determine the formation energies of *OCCOH on these four strong CO binding sites in Figure 3: 0.82, 0.56, 0.61, and 1.08 eV, for A to D respectively. These energies can be compared to our predicted formation energy from Grand Canonical QM and full solvent QM based metadynamics that led to a 1.01 eV barrier for *OCCOH on the Cu (111) surface and 0.70 eV on the Cu (100) surface. The first three sites (A, B, C) have *OCCOH formation energies lower than that for the Cu (111) surface. But site D has the highest formation energy of *OCCOH, even though it leads to the strongest CO binding site.

The B and C sites have *OCCOH formation energies lower than that for the Cu (100) surface, which indicates that these sites may provide better C−C coupling performance than the Cu (100) surface known to promote C−C coupling. We see that the common feature in these two sites is that at least one

under-coordinated neighbor square site exists along with the strong CO binding site, leading to the formation of the C−C bond in *OCCOH (as shown in Figure 3N and 3O). That is, of the four strongest CO binding sites, two lead to good CORR performance.

The two CORR active sites exhibit a common feature: an under-coordinated surface square site as shown in Figure 3B and 3C. Thus, CO binding energy alone is not a sufficient descriptor to identify sites favorable for ethanol production. Instead, we need a strong CO binding site on under-coordinated square sites that can facilitate *OCCOH formation.

To validate this conclusion, we propose in Figure 4 a small periodic cell (4 by 4 supercell) for the Cu surfaces that contains
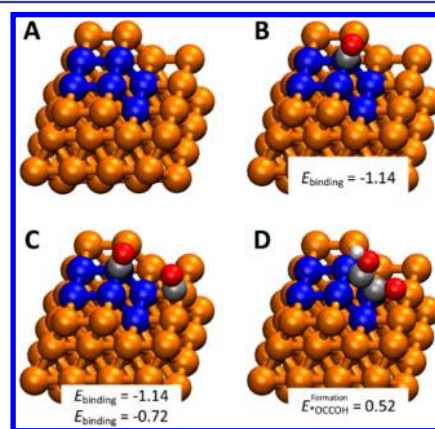
Figure 4. (A) Atomic structure of Cu surface site proposed to favor binding to *OCCOH and hence product ethanol. This has a strong CO binding site next to a weak binding site around a square surface configuration. (B) The surface bonded CO to the site in A. (C) two surface bonded CO bound to the site in A, and (D) the surface bonded *OCCOH. The colors are Cu in orange, C in silver, O in red, and H in whites. The closest Cu binding sites are shown in blue for viewer convenience. Experimentally, these active sites survive under CO2RR conditions (for at least 14 h).[18]

the features we found to be important on the NP. Figure 4A leads to two CO binding sites on this surface: one with a strong binding energy of 1.14 eV and one with a weaker CO binding energy of 0.70 eV. Our previous QM metadynamics calculations with full solvent showed that a CO binding energy of 0.70 eV is sufficient to keep CO on the surface at potentials less negative than −0.91 V (RHE).[15] We find that this combination of binding sites reduces the *OCCOH formation energy to 0.52 eV, which is the best performance among the active surface sites investigated here.

To experimentally identify active sites for C−C coupling, we propose using acetylene (C_2H_2) as a more specific probe than CO for such sites. Despite the different molecular orbital couplings, both of *OCCOH and chemisorbed C_2H_2 show preference for square sites. The structure of HC≡CH bonded to the surface has H−C−C bond angles of ∼120°, leading to an sp^2 orbital on each C that bonds to a metal site. For O≡C−C−OH, the left C has one electron in an sp^2 orbital that bonds to the Cu, while the other carbon makes more of a carbene bond to the surface. Thus, a C_2H_2 probe should provide a far better correlation to activity for C2 based product production than CO (Figure S5B).

To summarize, we computationally synthesized a Cu NP (158,555 atoms) deposited on a CNT reaching the size of the

experiment catalyst with a nominal thickness of about 10 nm. The predicted XRD pattern confirms the FCC structure of the Cu NP, which is consistent with experiment. The predicted TEM images and dislocation analysis show the GBs on this Cu NP. To search for the active sites, we randomly selected 5‰ of the surface sites for DFT calculations of the CO binding energies and found that 9% of the surface sites have binding energies larger than the low index surfaces, (111), (100), and (211). These strong binding sites explain the experimental TPD desorption peak at 273 K. We found that not all strong CO binding sites are active for C2 formation. Instead, only the strong CO binding sites with at least one under-coordinated neighbor square site can promote C−C coupling. According to these observations, we propose a periodic structure of metallic copper with continuously stepped square sites that may provide the best catalytic efficiency toward C−C coupling, which could serve as a prototype for catalysis design. We demonstrate that combining theoretical calculations (ReaxFF and QM) with experimental observations allowed us to identify new active sites. As we accumulate such results from theory, we may be able to develop a sufficient understanding of nanocatalysis kinetics that we could use knowledge based methods (such as machine-learning models basing on geometries) to explore all surface sites.

■ ASSOCIATED CONTENT

Ⓢ Supporting Information

The Supporting Information is available free of charge on the ACS Publications website at DOI: 10.1021/jacs.7b03300.

> Additional discussion of simulation methods, energy convergence benchmark for cluster calculations and ReaxFF (Cu/C) force field (PDF)

■ AUTHOR INFORMATION

Corresponding Author

*wag@wag.caltech.edu.

ORCID Ⓞ

Tao Cheng: 0000-0003-4830-177X
Hai Xiao: 0000-0001-9399-1584
William A. Goddard: 0000-0003-0097-5716

Notes

The authors declare no competing financial interest.

■ ACKNOWLEDGMENTS

■ REFERENCES

(1) Schouten, K. J. P.; Calle-Vallejo, F.; Koper, M. T. M. *Angew. Chem., Int. Ed.* **2014**, *53*, 10858−10860.

(2) Gattrell, M.; Gupta, N.; Co, A. *J. Electroanal. Chem.* **2006**, *594*, 1−19.

(3) Kuhl, K. P.; Cave, E. R.; Abram, D. N.; Jaramillo, T. F. *Energy Environ. Sci.* **2012**, *5*, 7050−7059.

(4) Hori, Y. Electrochemical CO_2 Reduction on Metal Electrodes. In *Modern Aspects of Electrochemistry*; Vayenas, C., White, R., Gamboa-Aldeco, M., Eds.; Springer: New York, 2008; Vol. *42*, pp 89−189.

(5) Hori, Y.; Konishi, H.; Futamura, T.; Murata, A.; Koga, O.; Sakurai, H.; Oguma, K. *Electrochim. Acta* **2005**, *50*, 5354−5369.

(6) Peterson, A. A.; Abild-Pedersen, F.; Studt, F.; Rossmeisl, J.; Norskov, J. K. *Energy Environ. Sci.* **2010**, *3*, 1311−1315.

(7) Nie, X.; Esopi, M. R.; Janik, M. J.; Asthagiri, A. *Angew. Chem., Int. Ed.* **2013**, *52*, 2459−2462.

(8) Cheng, T.; Xiao, H.; Goddard, W. A. *J. Am. Chem. Soc.* **2016**, *138*, 13802−13805.

(9) Durand, W. J.; Peterson, A. A.; Studt, F.; Abild-Pedersen, F.; Nørskov, J. K. *Surf. Sci.* **2011**, *605*, 1354−1359.

(10) Carmo, M.; Fritz, D. L.; Mergel, J.; Stolten, D. *Int. J. Hydrogen Energy* **2013**, *38*, 4901−4934.

(11) Medina-Ramos, J.; DiMeglio, J. L.; Rosenthal, J. *J. Am. Chem. Soc.* **2014**, *136*, 8361−8367.

(12) Kortlever, R.; Shen, J.; Schouten, K. J. P.; Calle-Vallejo, F.; Koper, M. T. M. *J. Phys. Chem. Lett.* **2015**, *6*, 4073−4082.

(13) Schouten, K. J. P.; Kwon, Y.; van der Ham, C. J. M.; Qin, Z.; Koper, M. T. M. *Chem. Sci.* **2011**, *2*, 1902−1909.

(14) Schouten, K. J. P.; Qin, Z.; Gallent, E. P.; Koper, M. T. M. *J. Am. Chem. Soc.* **2012**, *134*, 9864−9867.

(15) Cheng, T.; Xiao, H.; Goddard, W. A. *Proc. Natl. Acad. Sci. U. S. A.* **2017**, *114*, 1795−1800.

(16) Cheng, T.; Xiao, H.; Goddard, W. A. *J. Phys. Chem. Lett.* **2015**, *6*, 4767−4773.

(17) Li, C. W.; Ciston, J.; Kanan, M. W. *Nature* **2014**, *508*, 504−507.

(18) Feng, X.; Jiang, K.; Fan, S.; Kanan, M. W. *ACS Cent. Sci.* **2016**, *2*, 169−174.

(19) Verdaguer-Casadevall, A.; Li, C. W.; Johansson, T. P.; Scott, S. B.; McKeown, J. T.; Kumar, M.; Stephens, I. E. L.; Kanan, M. W.; Chorkendorff, I. *J. Am. Chem. Soc.* **2015**, *137*, 9808−9811.

(20) Foiles, S. M.; Baskes, M. I.; Daw, M. S. *Phys. Rev. B: Condens. Matter Mater. Phys.* **1986**, *33*, 7983−7991.

(21) Redhead, P. A. *Vacuum* **1962**, *12*, 203−211.

(22) Vollmer, S.; Witte, G.; Wöll, C. *Catal. Lett.* **2001**, *77*, 97−101.

(23) Calle-Vallejo, F.; Koper, M. T. M. *Angew. Chem., Int. Ed.* **2013**, *52*, 7282−7285.

(24) Pérez-Gallent, E.; Figueiredo, M. C.; Calle-Vallejo, F.; Koper, M. T. M. *Angew. Chem., Int. Ed.* **2017**, *56*, 3621−3624.

(25) Xiao, H.; Cheng, T.; Goddard, W. A. *J. Am. Chem. Soc.* **2017**, *139*, 130−136.